International Journal of Biological Macromolecules 292 (2025) 139203

Contents lists available at ScienceDirect

International Journal of Biological Macromolecules

journal homepage: www.elsevier.com/locate/ijbiomac

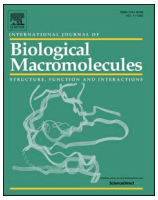

Multifunctional nanocellulose hybrid films: From packaging to photovoltaics

Joaquin Valdez Garcia [a], Anna Boding [b], Xuan Yang [c], Rustem Nizamov [a], Michael S. Reid [b,d], Kristina Junel [b], Kati Miettunen [a], Tiffany Abitbol [b,e], Joice Kaschuk [f,*]

[a] Department of Mechanical and Materials Engineering, Faculty of Technology, University of Turku, FI-20500 Turku, Finland
[b] RISE Research Institutes of Sweden, SE-114 28 Stockholm, Sweden
[c] State Key Laboratory of Chemical Engineering, Key Laboratory of Biomass Chemical Engineering of Ministry of Education, College of Chemical and Biological Engineering, Zhejiang University, Hangzhou 310027, PR China
[d] Department of Fibre and Polymer Technology, School of Engineering Sciences in Chemistry Biotechnology and Health, KTH Royal Institute of Technology, SE-10044 Stockholm, Sweden
[e] Sustainable Materials Laboratory, Institute of Materials, School of Engineering, EPFL, Station 12, 1015 Lausanne, Switzerland
[f] Physical Chemistry and Soft Matter, Wageningen University and Research, 6708 WE Wageningen, Netherlands

ARTICLE INFO

Keywords:
Cellulose nanofibers
CNF
Cellulose nanocrystals
CNC
Montmorillonite
MTM
Nanoclay

ABSTRACT

This study aimed to develop eco-friendly multifunctional nanocellulose (NC) hybrid films with tailored properties for versatile applications including packaging and photovoltaics. Hybrid films composed by cellulose nanocrystals (CNC) and carboxymethylated cellulose nanofibrils (CNF) were produced at various mass ratio (CNC - 100:0 to 0:100). Montmorillonite clay (MTM) was incorporated (50 % by mass) into the CNC:CNF films. CNC-only films easily dispersed in water, but by adding CNF or MTM, the structural integrity was enhanced. Films with ≥50 % CNF and MTM had a strength reduction of 9–35 % and increased brittleness. The hybrid films presented transmittance above 60 % and haze varying from 5 % to 60 % at 550 nm which can be a beneficial for light management. All films kept color stability over 1000 h of artificial sunlight, a critical packaging feature for long-term storage. CNC: CNF films without MTM showed better potential for optoelectronic applications due to higher transmittance and smoother surfaces, while those with MTM presented UV protection (up to 250 nm) and swelling resistance (28–53 %) which could also benefit optoelectronics increasing their lifespan. Balancing the hybrid films composition is key for optoelectronics, while packaging applications tolerate broader compositions. These findings demonstrate the versatility of NC hybrid films in creating sustainable materials for diverse applications.

1. Introduction

Several scientific discoveries have accelerated the development of our society; however, undoubtedly, one that had a profound impact was the discovery of the first synthetic plastic in 1907 [1]. The production of petroleum-based plastics increased with the unprecedented economic growth and the emergence of the modern consumer society, generating a vast amount of printed electronics and packaging [1,2]. This revolution has also come with environmental problems due to the uncontrolled disposal of these materials [3]. Now, the focus has shifted toward the search for eco-friendly and renewable materials that possess sufficient characteristics as alternatives to high-performance products developed by synthetic plastics [4]. In this scenario, scientists are revisiting well-established technologies and materials, such as paper, first processed in 105 CE [5], as an alternative, promising material for printed electronics and packaging. Paper and related products have a long history in information storage/exchange and packaging [4]. However, lately these materials have been reimagined in the nanotechnology sector to broaden their scope and utility into a wide range of applications.

Nanocellulose (NC) can be used to produce films with high oxygen barrier and high transparency, which are attractive features for packaging and optoelectronics, respectively [6,7]. NC is often categorized into cellulose nanocrystals (CNC), cellulose nanofibrils (CNF), and bacterial cellulose. CNC present highly crystalline, short, and rod-shaped structures, whereas CNF is longer, and can be thread-like and discrete, or sometimes entangled or branched [8]. Their different

* Corresponding author.
E-mail address: joice.kaschuk@wur.nl (J. Kaschuk).

https://doi.org/10.1016/j.ijbiomac.2024.139203
Received 12 July 2024; Received in revised form 19 November 2024; Accepted 23 December 2024
Available online 25 December 2024

morphologies lead to films with distinct properties, for instance, CNC films are generally brittle, with low tensile strength and high Young's modulus, while CNF films offer more flexibility and a higher tensile strength [9].

Additionally, alterations in the swelling ability of NC films have been studied by the production of hybrid films containing nanosized layered minerals known as nanoclays [10]. The most used nanoclay is montmorillonite (MTM), which has an exfoliated nanoplatelet thickness of 1 nm and a lateral size ranging from 30 nm to several μm, along with a net negative surface charge [11]. So far, only hybrid materials composed of CNF and MTM have been reported [12–15], and all properties are dependent on the dispersibility of the main components in suspension before film formation. Overall, after the formation of the hybrid film, a layered structure is observed, consisting of an ordered platelet packing surrounded by a nanocellulose matrix [6]. This configuration not only results in improved water and oxygen barrier performance [16] but also serves as an additive for flame retardation [17].

This study was developed in the application contexts of (1) packaging and (2) solar cells, where key properties are crucial for the performance of these materials. For instance, an ideal packaging film material should exhibit sufficient mechanical and barrier properties, where the required levels depend on product specifications [18]. For packaging, optical transparency may not be required, whereas features such as water resistance might be essential. On the other hand, for solar cell substrates, the critical requirement is high transparency, followed by adequate mechanical properties, low roughness, and water resistance. Additional optical properties, such as antireflection, can improve solar cell performance [19]. Lastly, UV-blocking is a property that can enhance performance in both applications [20,21]. Obtaining all these features from biobased materials is a challenge.

Herein, we mitigate strategies for improving the properties of CNC films. The first approach was to study the formation of hybrid films containing only CNC and MTM, which remains unexplored. Followed by the production of tri-component hybrid films composed of CNC, CNF, and MTM. The idea of adding CNF to the system comes from the tunability of optical, mechanical, and thermal properties reported in the following research paper [9,22–25]. For the films with the most promising properties for optoelectronics application, we additionally investigated the stability under artificial sunlight, their angular light transmittance, and their surface structure. This study provides insights into the interactions between CNC, CNF, and MTM, laying the groundwork for new customized materials tailored for applications in packaging and photovoltaics.

2. Methodology

2.1. Materials

Spray-dried CNC in Na-form (CelluForce) was mixed into a 2 wt% aqueous CNC suspension using a Vibracell probe sonicator (probe 219–07), followed by filtration through Munktell #3 filter paper. This CNC is highly characterized elsewhere [26], including size and zeta potential.

Carboxymethylated CNFs were produced in-house from a commercial, never-dried, bleached softwood sulfite dissolving pulp (Domsjö Fabriker AB, Sweden) [27]. To obtain CMC-CNF, the carboxymethylated pulp was passed once at 1700 bar through and pilot-scale homogenizer (Microfluidizer M-110EH, Microfluidics Corp., United States). The CNF had a degree of substitution (DS) of 0.1 (600 μeq/g) and a concentration of 2.18 wt%. At pH $>$ 6, the charge groups of the CNF are dissociated, and the samples are colloidally stable, at pH $<$ 6, the charge groups are protonated, and colloidal stability is compromised. In the current work, everything was done at neutral pH, where CNC and CNF are colloidally stable [28].

The sodium montmorillonite clay (MTM), also called Cloisite-Na^+ was donated by BYK. MTM was added as a powder to the NC suspensions, with magnetic stirring overnight to promote a uniform dispersion. As MTM was not colloidally stable, we could not measure zeta potential on such a system.

2.2. Methods

2.2.1. Film preparation

Films (25 $g{\cdot}m^{-2}$) consisting of CNC and/or CNF, with and without MTM, were prepared by solvent casting (Fig. 1). The suspensions were stirred overnight, poured into polystyrene Petri dishes, and dried at 23 °C in a 50 % relative humidity environment. The CNC: CNF films were prepared at mass ratios of 100:0, 75:25, 50:50, 25:75, and 0:100, and the films containing MTM consisted of 50:50 cellulose (CNC: CNF): MTM by mass (Table 1).

After air drying at 23 °C and 50 % RH, all the films were dried for an additional 1 h at 150 °C. One film from each system was placed in a frame to dry under tension, first at 23 °C and 50 % RH, followed by 1 h at 150 °C. The film dried under tension was used for subsequent mechanical analysis, where it is important that the films are not wrinkled.

2.2.2. Characterization

2.2.2.1. NC and MTM morphology. The morphology of CNC, CNF and MTM was characterized by atomic force microscopy (AFM; Multimode 8 in ScanAsyst mode; SCANASYST-Air cantilevers). Suspensions of CNC: CNF (100:0, 50:50, and 0:100) with and without MTM were spin coated at low concentration (0.02–0.025 wt%) onto silicon wafers that were pre-coated with polyethyleneimine (PEI) at 1 g/L.

2.2.2.2. Suspension properties. The rheological behavior of CNC (2 and 4 wt% suspensions) and CNC: MTM mixture (2 wt% each) were measured using a Malvern Kinexus Pro rheometer in a cone-plate configuration, with a PL65 S1240 SS lower plate and a CP4/40 SR0734 SS upper cone.

2.2.2.3. Film properties. The *mechanical properties* of the hybrid films were measured by tensile tests using an MTS 3125 tensile tester, where the span length and sample width was set at 30 mm and 6 mm, respectively. Note that all the samples were conditioned at 50 % RH and 23 °C before the tests. Optical properties were evaluated from 200 to 800 nm using the Diffuse Reflectance Accessory coupled to UV–Vis-NIR Agilent Cary 5000 from Agilent Technologies. The *structure and morphology* of the films was evaluated by polarized optical microscopy (Zeiss Axioplan polarized optical microscope with 540 nm waveplate) and scanning electron microscopy (SEM, Hitachi S-4300, Japan).

The *water sensitivity* of the films was initially evaluated using a fast swell test where a piece of film was immersed in water and vortexed for 20 s, comparing film appearance/thickness from digital photographs.

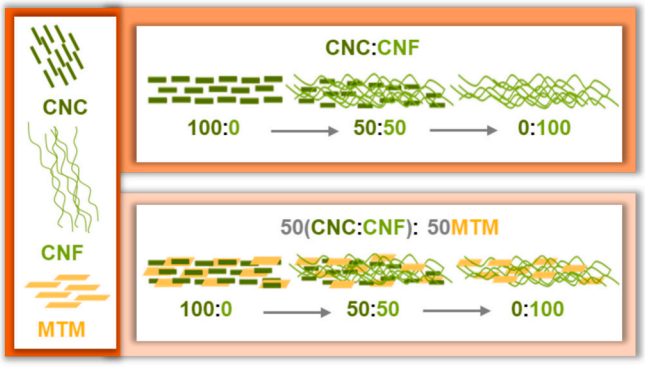

Fig. 1. Schematic of production of films produced from cellulose nanocrystals (CNC), cellulose nanofibrils (CNF), and montmorillonite (MTM).

Table 1
Composition of the films. CNC and CNF were mixed to make NC suspension (their percentages are below). Then, to study the impact of clay, we added MTM to NC suspension, and the table gives the percentage of its mass compared to the total mass of dry matter (CNC, CNF, and MTM) in the final solution.

	CNC	CNF	MTM
100CNC:0CNF	100	0	0
75CNC:25CNF	75	25	0
50CNC:50CNF	50	50	0
25CNC:75CNF	25	75	0
0CNC:100CNF	0	100	0
100CNC:0CNF-MTM	100	0	50
75CNC:25CNF-MTM	75	25	50
50CNC:50CNF-MTM	50	50	50
25CNC:75CNF-MTM	25	75	50
0CNC:100CNF-MTM	0	100	50

Then, traditional swell tests were performed by evaluating the difference between the initial film thickness measured using a digital caliper and the final thickness of water-swollen films at different time points (30, 60, 120 min, and overnight). For select films, water vapor transmission rates (WVTR) were measured on film areas of 5 cm^2, following the ASTM F 1949–13 standard using AMETEK - MOCON Inc., Minneapolis, MN, USA Instrument PERMATRAN-W® 3/31 MG WVTR analyzer.

The *angle-dependent transmittance* of the hybrid films was determined using an integrating sphere device (Artifex Engineering 100 mm Integrating Sphere), couple with a motorized rotating stage to ensure the measurements at different angles. A Thorlabs SL201L/M Stabilized Tungsten-Halogen Light Source, and a Thorlabs CCS200/M compact Czerny-Turner spectrometer were used, in which wavelength of 500–900 nm was collected with a 2 nm interval.

The *stability of the films under artificial sunlight exposure* was performed using artificial sunlight (1 Sun both visible and UV, corresponding to the AM1.5G spectrum) with the aid of the Atlas XLS+ solar simulator chamber with a xenon lamp (model NXE 1700 with light spectrum reported in reported in [29] for 1800 h. The total irradiation exposure in the 300–400 nm wavelength range was approximately 430 MJ/m^2. The ambient temperature inside the simulator chamber was 35 °C and the relative humidity was 10 %. The temperature of the samples measured with the Fluke TiS75 thermal imaging camera was around 45 °C. The visual tracking of film changes was conducted using a process described in [30,31]. This included using a dedicated

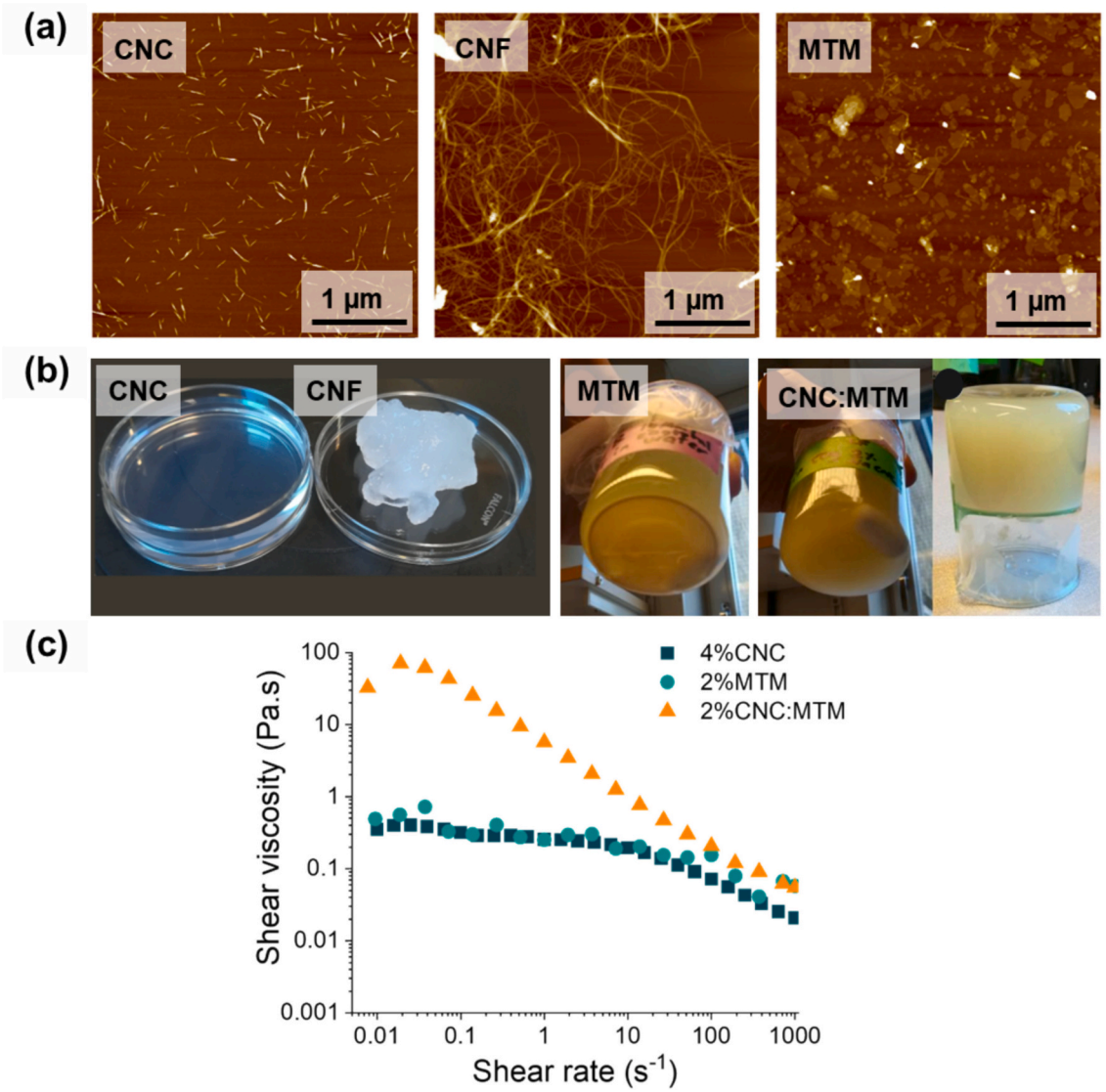

Fig. 2. (a) AFM images of CNC, CNF, and MTM, (b) photographs of CNC and CNF suspensions at 4 and 2 wt%, respectively, MTM at 2 wt% in water showing sedimentation, and CNC and MTM mixture showing a uniform gel-like suspension that resists flow upon sample inversion, (c) shear-viscosity of neat MTM (2 wt%), neat CNC (4 wt%), and mixtures of CNC and MTM, each at 2 wt.

photography chamber, specific camera settings, and an X-Rite ColorChecker Passport for accurate color representation. The analysis of the color changes through the average red, green, and blue (RGB) values across three different non-reflecting regions was conducted using a Python (3.9) script. These areas were selected to yield an average color value that closely represents the actual color of the CNC: CNF films.

The *surface roughness* of the CNC: CNF films (25 μm^2 area) was analyzed by AFM (Park Systems NX10, scanning 256 pixels). The measurements were done on the side of the film in contact with the Petri dish when cast, as this side is usually smoother [32]. For comparison, samples of polyethylene terephthalate (PET, Melinex 505, Pütz Folien) and polyethylene naphthalate (PEN, Teonex Q65HA, Pütz Folien) were also evaluated. The images were analyzed using Gwyddion 2.60. AFM images were all leveled first by mean plan subtraction, then fitted with a second-order polynomial and minimum values set to zero.

3. Results and discussion

3.1. Suspension physical characteristics

As a starting point, all the nanomaterials have very different shapes (Fig. 2a): from short rigid rods (CNC) to long slender fibrils (CNF), and nanoplatelets (MTM). In suspension form, they are all negative charged with sodium counterions, leading to totally different suspension states. For instance, at 4 wt%, CNC suspensions are liquid, whereas CNF yields a highly entangled gel already at 2 wt% (Fig. 2b) due to its higher aspect ratio and surface charge. MTM suspension at 2 wt% developed a powdery sediment, especially after several days left undisturbed (Fig. 2b), likely due to insufficient exfoliation and unexfoliated aggregates remaining after overnight magnetic stirring without fractionation [33].

Interestingly, when CNC and MTM were combined (total solids 4 wt %; 2 wt% CNC and 2 wt% MTM), a uniform gel-like consistency was obtained, stiff enough to resist flow upon inversion of its container (Fig. 2b), which was furtherly confirmed by the shear-thinning behavior (Fig. 2c). This may be attributed to the promoted MTM exfoliation by adding colloidal stable CNC nanoparticles with potential entropic interactions where water is released from the surface upon adsorption, which could favor different interactions, including van der Walls and hydrogen bonding between the cellulose surface and MTM in the films [34,35]. Similarly, CNF: MTM hybrid suspension also demonstrates high colloidal stability. Overall, pristine CNC and CNF hybrid NC/MTM suspensions are all colloidal stable, guaranteeing a homogeneous formation of film materials using a solvent casting process.

3.2. Film formation and structure

The hybrid films were cast by water evaporation under controlled 50 % humidity and 23° C temperature to promote slow and uniform self-assembly. The total grammage of the films was maintained at 25 $g{\cdot}m^{-2}$, aiming for their homogeneity, thickness, and density (as detailed in Table S1). Despite that, as the composition of an NC was altered, changes in these characteristics were observed, mostly probably regarding the particles' self-organization and interactions between the different materials during the films' drying process. Changes in the density of the films were mainly impacted by the film thickness. This happened because the density was calculated from the relation between the volume (thickness x $1cm^2$ area) and weight of the sample (method description added to SI). For instance, CNC has short length and could fit more in the voids caused by the CNF fibers. In the other hand, adding MTM, which has different chemical structure compared to CNC and CNF, intensifies the alterations. While there are these variations, it should be noted that the density of sample containing only CNF is comparable with our previous studies [36]. Additionally, the porosity (Eq. S1) of nanocellulose films refers to the relationship of density of the nanopaper with the density of cellulose fibers (1.46 $g.cm^{-3}$). This equation presents limitations, once our system is not composed by only nanocellulose but also nanoclay. When this equation is valid, we have very low porosity ranging from 0 to 36 % (Table S1) in agreement with previous research [37].

As expected, neat CNC films (100:0) presented a homogenous structure with a special chiral nematic assembling character (POM images and SEM images in Fig. 3). By mixing with CNFs with increasing contents, the POM images became dominated by birefringent cellulose microfibrils, appearing blue and yellow depending on their direction. Similarly, the chiral character is lost in the SEM image (50:50), with the mille-feuille layers typical of CNF prevailing.

The addition of MTM into a neat CNC film (100:0) led to films with a very low light twisting (no birefringence in Fig. 3 POM image), but with a highly organized layered structure (Fig. 3 cross-sectional SEM). This absence of birefringence indicates a highly planar organization, near-perfect parallel to the plan of the film/perpendicular to the viewing direction. This has been termed a "brick and mortar" structure for NC: MTM hybrid films [38]. When CNF was included, the layered structure persisted. However, large gaps appeared between layers, attributed to microfibrils and cellulose fibrils interrupting the structure. Finally, we note that, in general, the POM images of the films containing MTM were darker due to the higher opacity of MTM.

3.3. Tensile properties

CNC are rigid rod-like particles, which translates to rigid CNC films with inferior flexibility due to the limited entanglements and interparticle bandings resulting in poor tensile properties [39]. No significant changes in their tensile properties were observed by adding MTM to neat CNC film (Fig. 4, cross-hatched bars). Furthermore, inspired by previous reports [9,22–25], the addition of CNF into CNC led to a linear increase on strength values and decrease of Young Modulus. Meaning that the long flexible CNF acted as a plasticizer modifying the tensile properties due to the entanglement of the fibrils within the structure and creating more elastic materials [40,41]. Additionally, CNC bridge the gaps between CNF acting as physical crosslinking and extend the NC network [25]. After adding MTM which presents different shape and chemistry, the hybrid films containing 75CNC:25CNF (Fig. 4) presented a higher strength value compared to the film without MTM. For the films containing higher CNF content, the presence of MTM in the hybrid films induced an interruption to the NC network, decreasing their strength. The MTM interruption induced an increase in the brittleness of all the films. Furthermore, no clear correlation exists between the films' strength and density (Table S1).

Comparing results from the literature proves challenging for several reasons. Alterations in the NC's dimensions and its surface chemistry adversely affect the tensile performance of hybrid films, as observed at Table 2. However, it was possible to observe the similarity in our strain at break values with those hybrid films found in the literature, even though the composition was not similar. There is a notable oversight in recognizing CNC's role in these systems. There are no reports of hybrid films containing only CNC and MTM. Hybrid systems containing CNC: CNF are found [9,22–25], showing that hybrid materials containing CNC exhibit inferior mechanical properties compared to films solely composed of CNF and MTM, as described in Table 2. Therefore, it is suggested that CNC has more impact than MTM on hybrid film properties.

3.4. Water interactions: swelling and water vapor transmission

Cellulosic materials generally have poor water vapor barrier properties due to their hydrophilic surface with abundant hydroxyl groups [8]. Such effect is often amplified for NC, since CNC and CNF are often obtained with -SO_3H or -COOH groups and present greater surface area [8]. Understanding the impact of the water interactions within the hybrid materials here is a critical aspect in the framework of applications; for instance, this feature is often important for packaging and

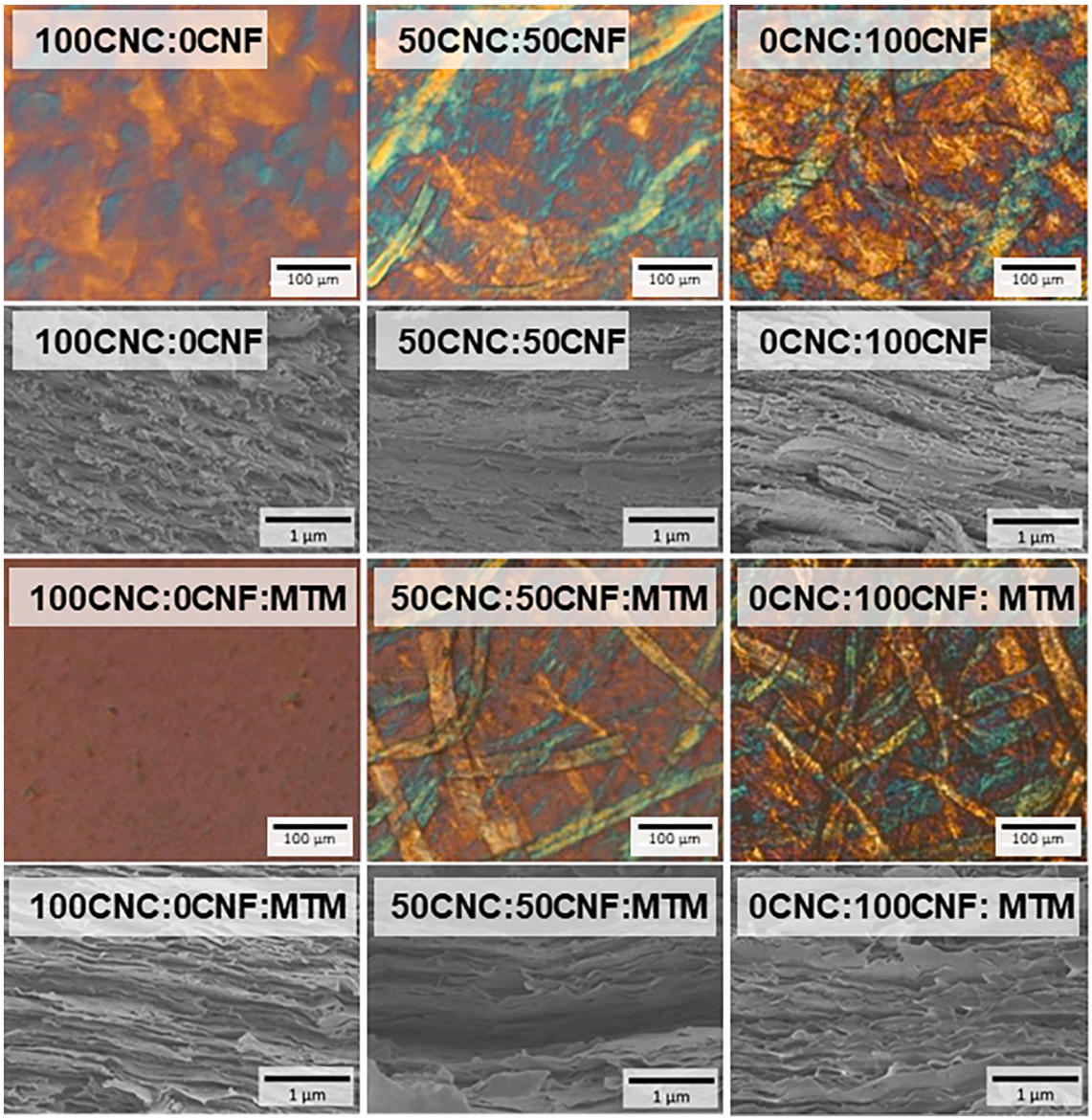

Fig. 3. Polarized optical microscopy (POM) (first and third row) and scanning electron microscopy (SEM) (second and fourth row) images of the hybrid films.

substrates for optoelectronics.

During our initial experiments, it was noticed the films mostly swelled in the thickness direction. For this reason, it was decided to perform the evaluation of swelling of the films by measuring the differences between the thickness before and after immersing in water. The Table S2 shows all the thickness measurements at diverse times, and there is a consistency on the results, then, it was opted to present only the time 24 h in the core text. Additionally, similar method was already used by other researchers to evaluate the swelling behavior, please see [46,47].

As a baseline, neat CNC films are completely dispersed upon immersion in water for only 30 min without any agitation due to the enhanced swelling effect of CNC particles and the network structure, which has minor entanglements [48]. Mixing CNF or MTM into CNC, the obtained hybrid films presented lower swelling behavior (Fig. 5a). By adding CNF into CNC, the fibre entanglement commonly observed in CNF films is translated to the hybrid films holding CNC together within its structure. Additionally, films with a higher CNF content are expected to swell more since the ionic swelling pressure will increase with CNF and its higher charge density. For the CNC: MTM film, the decrease in swelling could be attributed to the highly regular stratified structure formed by CNC intercalated with parallel nanoplatelets of MTM (Fig. 3), reducing water interactions, which is again supported by the "brick and mortar" structure [38].

Consequently, by combining CNC, CNF, and MTM, it was possible to achieve even lower swelling (Fig. 5) and higher density values (Table S1), indicating that the synergy among these components can be harnessed to produce materials with reduced water uptake. Notably, the hybrid material with the lowest swelling behavior comprised MTM and 75CNC: 25CNF, which also presented the highest density (1.71 $g.cm^{-3}$). Additionally, the visual appearance of the thickness and swelling of the films is presented in Fig. 5b. Herein, the films containing MTM (1 and 3) presented lower thickness, indicating lower swelling than those without MTM (2 and 4). This coincides with the thickness values obtained during the swelling tests (Table S2).

In addition, we evaluated the water vapor transmission rate (WVTR) for the 50:50 and 0:100 CNC: CNF films, both with and without MTM. The results of the WVTR measurements are found in Table 3. Please note that the WVTR values presented are based on a single measurement per sample and should be considered indicative of how the sample would behave. Furthermore, we were unable to measure the 100:0 CNC: CNF films, both with and without MTM, due to the presence of small cracks in

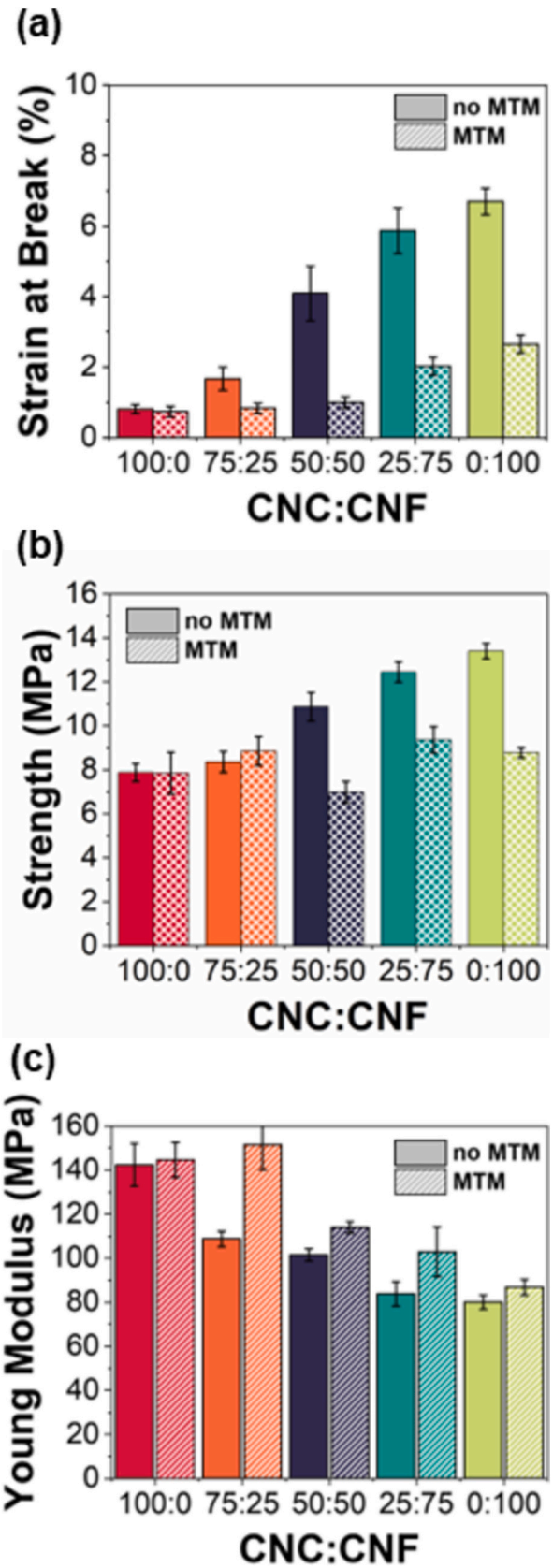

Fig. 4. Mechanical properties: (a) strain at break, (b) strength, and (c) young modulus of CNC: CNF films with and without MTM. The error bars represent the standard deviation of seven samples.

Table 2
Comparison of tensile property values of NC-MTM hybrid films in literature and this study. All films have a 50:50 NC-MTM dry mass ratio.

NC-MTM 50:50	Strain at failure (%)	Strength (MPa)	Young modulus (GPa)	Thickness (μm)	Ref.
HoloCNF-MTM	2.2 ± 0.3[a] 0.7 ± 0.1[b]	243.7 ± 11.5[a] 193 ± 26[b]	30.1 ± 1.3[a] 34.8 ± 2.3[b]	30	[42]
TOCNF-MTM	4.3 ± 0.2	420 ± 19	19.4 ± 2.9	5–7.7	[43]
TOCNF-MTM[c]	1.0 ± 0.1	313.60 ± 22.92	38.4 ± 3.3	30	[12]
CNF-MTM	1.3 ± 0.3	214 ± 16	27.8 ± 1.7	35–40	[44]
a. QCNF-MTM b. TOCNF-MTM	a. 4.6 ± 0.9 b. 1.7 ± 0.2	a. 138 ± 20 b. 236 ± 13	a. 16.7 ± 2.1 b. 21.8 ± 3.5	~40	[15]
CNF-MTM	2.8 ± 0.2	123 ± 4	7.5 ± 0.2	60–80	[45]
100CNC:0CNF-MTM	0.7 ± 0.1	8 ± 1	14.4 ± 0.8	23 ± 7	Our work
75CNC:25CNF-MTM	0.8 ± 0.1	8.9 ± 0.7	15 ± 2	17 ± 3	
50CNC:50CNF-MTM	1.0 ± 0.1	7.0 ± 0.5	11.4 ± 0.3	22 ± 3	
25CNC:75CNF-MTM	2.0 ± 0.3	9.3 ± 0.6	10 ± 2	25 ± 3	
0CNC:100CNF-MTM	2.7 ± 0.3	8.8 ± 0.2	8.7 ± 0.4	26 ± 3	

QCNF: quaternary ammonium cellulose nanofibrils; TOCNF: Tempo oxidized cellulose nanofibrils.
[a] Components suspended in water at same time.
[b] Components dispersed in suspension prior mixture.
[c] 53.8 % MTM.

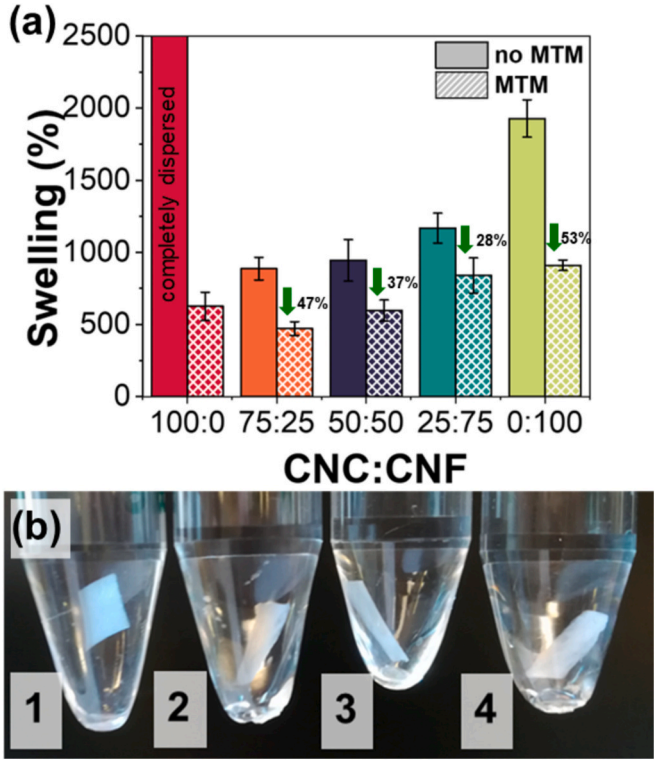

Fig. 5. Swelling tests of the hybrid materials. (a) Swelling percentage of the hybrid materials containing CNC, CNF, and MTM after 120 min (equilibrium), Note: the decreasing percentage values presented are related to the difference between CNC: CNF without MTM and with MTM. (b) Digital photographs of hybrid films after being rapidly agitated by vortex for 20 s: (1) 50:50: MTM, (2) 50:50, (3) 0:100: MTM and (4) 0:100 CNC: CNF films.

Table 3
Water vapor transmission rate (WVTR) of select films containing CNC, CNF, and MTM. Measurements were conducted at 23 °C and 50 % relative humidity.

CNC: CNF	Thickness (μm)	WVTR (g/m^2·day)	WVTR (g·mm/m^2·day)
50:50	22.9	144.2	3.3
50:50: MTM	18.6	133.1	2.4
0:100	30.9	76.57	2.4
0:100: MTM	23.9	90.38	2.2

these brittle films, which made them unsuitable for WVTR testing. Overall, adding MTM in the hybrid materials reduces water vapor permeability, with a slightly more significant reduction observed for the CNC film. Indeed, it has been established by others that films based on CNC and MTM exhibit a significant decrease in WVTR values [49,50] however, we did not find similarly studied CNC: CNF: MTM hybrid films in the literature. Finally, we note that while these are only single values for WVTR in each sample, it is still evident that the WVTR values presented in Table 3 are insufficient for applications with high moisture barrier requirements, e.g., packaging materials where they intend to keep the product with low moisture content, or electronics.

3.5. Optical properties

NC films are known for their opacity, which is caused by the difference of refractive indexes between the fibers and the air [51]. In a single component system, the density is one of the factors that can influence the optical properties as observed in our previous publication [36]. However, with hybrid materials, analysing the impact of different properties to optical performance becomes more complicated. For instance, in this work, films composed of two nanocellulose sources demonstrate different optical properties compared to those with just a single component. These changes become even more significant when the inorganic compound (MTM) is added to the film.

Herein, the main visual appearance is related to the presence of MTM, which is observed in yellow shades in the films, as shown in Fig. 6. Regarding the UV–vis measurements, the neat CNC film had a distinct optical profile (Fig. 7a) due to a chiral nematic reflection (appearing as a broad valley in transmission at >450 nm), which disappeared with the slightest addition of CNF at 25 %. The CNC: CNF films have an overall transparency of >80 % (at 550 nm). However, the inclusion of larger

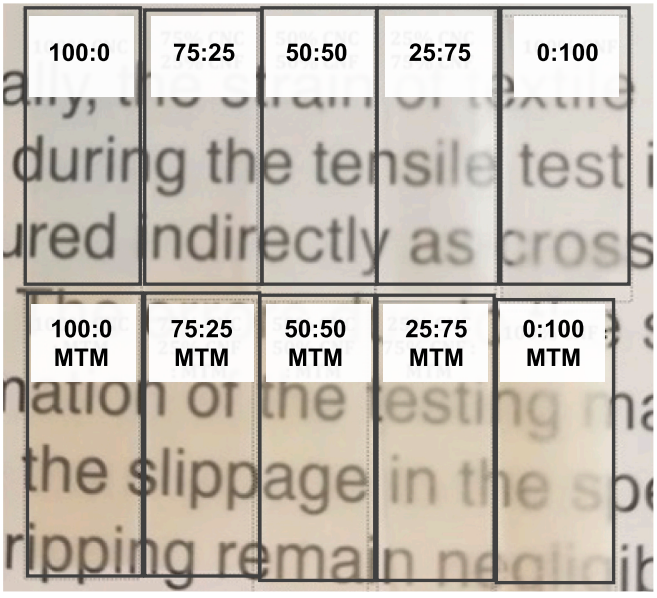

Fig. 6. Digital photographs of the hybrid films CNC: CNF containing MTM or not.

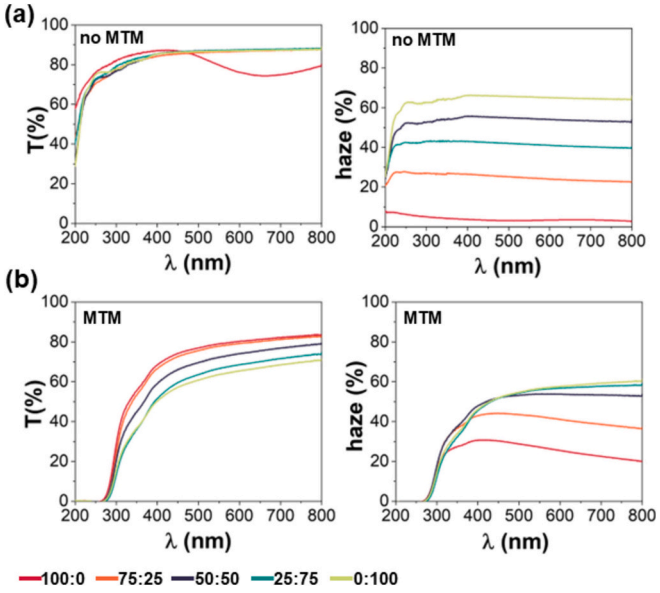

Fig. 7. Optical properties of (a) CNC: CNF films without and (b) with MTM.

microfibrils (with CNF content) that do not pack as uniformly results in the formation of very small air voids within the film, causing light scattering and haze (percentage of the light transmitted at an angle >2.5° from the direction of the incident beam) [51]. Here, the neat CNC film (100:0) had the lowest haze due to its homogenous structure and regular packing (Fig. 7a). Thus, as CNF is introduced into the film structure, gaps between layers and more air voids occur, leading to a higher optical haze (Fig. 7a).

With added MTM, the films with higher CNC content (100:0 and 75:25) exhibited the highest transparency and lowest haze, which may be attributed to a more uniform structure in these films (Fig. 3). As the CNF content was increased in the films containing MTM, transparency decreased (Fig. 7b). Adding MTM increased the haze in films with higher CNC contents (100:0 and 75:25). However, the haze values for 50:50 films were similar to those without MTM. It is not clear whether MTM had an impact on the haze values of the films with higher CNF contents, perhaps indicating that CNF dominated the effect. These results can be challenging to interpret, especially in multicomponent films, since they are influenced by many properties such as density, morphology, and thickness, as well as the optical properties, including refractive indices differences between the components of the films and air voids. For instance, in the neat CNC film, when MTM is added, the thickness increases (Table S1) and positively impacts the haze without changing the transmittance (Fig. S1). When MTM is added to CNF neat film, the density increases significantly (Table S1), decreasing both transmittance and haze (Fig. S1). Additionally, the inorganic character of MTM could also be why the transparency of the films was lower than those without it.

Although the addition of MTM leads to a significant decrease in water uptake, it also leads to a decrease in transparency, which hinders optoelectronics applications. In photovoltaics, it is important to have high transmittance at different angles to profit from all the incoming light. CNC: CNF films without MTM were selected to analyze the transmittance at different angles.

Thus, the transmittance of NC films was measured at different incidence angles. With an increasing angle of incidence, all films exhibited a decrease in transmittance (Fig. 8). This decrease indicates that the films either reflect or absorb a more significant portion of the incoming light. Films containing CNF exhibited a significant decrease in transmittance as the incidence angle increased, in contrast to the neat CNC film (100:0). Besides, the films with 50 % CNF or higher demonstrated a slightly lower overall transmittance with a faster and more pronounced

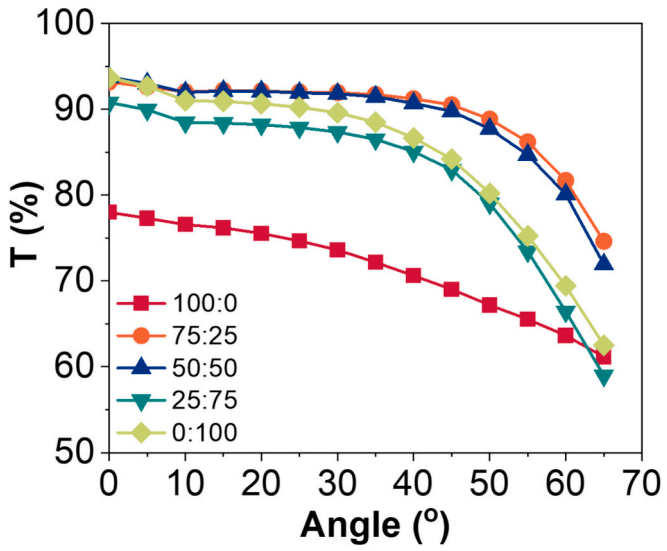

Fig. 8. Angle-dependent transmittance for CNC: CNF films from 0 to 65°. Each point is obtained by comparing the light transmitted by the film at a certain angle with a reference measurement without any obstructions. Afterward, this curve is compared to the solar spectrum to obtain a solar-weighted average and integrated to obtain a total transmittance value. Only wavelengths between 500 and 900 nm are considered.

decrease on the transmittance with the light angle changes. For the neat CNC films, at higher angles, there was a significant increase in the reflection of wavelengths ranging from 500 to 700 nm and a blueshift in the position of the valley, indicating the maximum reflection wavelength (Fig. S2). This was due to the iridescence of chiral nematic peaks, which show an angular variation due to the color/wavelength of the structure.

High haze in NC films has been associated with antireflection properties in literature. For instance, Fang et al. measured an increase in photocurrent at high angles (15 % increase between 60 and 87°) in a solar cell coated with hazy cellulose (haze≈60 %) [52]. They hypothesized that this increase was due to an increased pathway of the light in the active layer of the solar cell due to the haziness of the cellulose film. Here, both 50:50 and 0:100 CNC: CNF films exhibit high haze, yet they failed to reach higher transmittances at high angles (Fig. 8). Haze can increase the light path length, but decreasing the total transmitted light would reduce the generated photocurrent. Our results indicated that films with high haze would prevent light from entering the active area instead of improving its transmittance. While NC can be used to texturize a surface to be anti-reflective, high haze and transmission at high angles are not linked based on these results. Achieving good antireflection properties using films with high haze may require further refractive index engineering, which could cause the discrepancy between the work of Fang et al. and the current study.

3.6. Color stability under artificial sunlight

In applications such as optoelectronics, where high transparency or packaging, where long-term storage without discoloration is aimed, it is also critical how the materials withstand irradiation. Therefore, the color stability of CNC: CNF films under artificial sunlight exposure were studied by tracking the visible color changes on the films (Fig. 9). The neat CNC film (100:0) was left out of the testing since its robustness was insufficient to withstand the strain caused by the test. Additionally, CNC: CNF: MTM films were excluded due to their negative attributes of lower transparency and higher haze.

The color stability evaluation is commonly used in the photovoltaic field [29,53–56]. As an example, dye solar cells' stability and performance can be evaluated by the correlation between color changes and device power conversion [57]. A typical light soaking test in photovoltaics lasts 1000 h, [58] corresponding to a year in central European outdoor conditions [59]. Herein, the samples were aged until 1800 h, which corresponds to approximately 2 years in natural solar conditions [59]. In this analysis, the 8-bit RGB color space format presents three color channels in a range of 0 to 255. The RGB (0,0,0) combination results in the color black and the RGB (255, 255, 255) in the color white.

The CNC: CNF photos taken before and after the light were strikingly similar (Fig. 9). Therefore, all RGB channels remained unchanged during the light soaking test with minor color channel fluctuations for 75:25 CNC: CNF, which could be caused by high surface reflection due to minor changes in the positioning of the samples in the film holders. Ultimately, the CNC: CNF hybrid films presented high color stability, which is beneficial for photovoltaics and agrees with our previous studies [30,60,61].

3.7. Surface morphology

The roughness and the overall profile of the hybrid all-NC films were evaluated using AFM (Fig. 10). The smoothest film, with a root mean square (RMS) roughness of 17 nm, was obtained from the neat CNC film (100:0) (Fig. 10a). It was followed by films composed of 25: 75, and 50:50 CNC: CNF ratios, which exhibited RMS roughness values of 89 and 91 nm, respectively (Fig. 10d, c). Films comprising 75:25 and 0:100 CNC: CNF ratios had the highest roughness values of 123 and 229 nm, respectively (Table S3). As reported in a previous study [9], combining CNC and CNF can produce smoother films than pure CNF films. This is attributed to the ability of CNC to form denser films rather than a porous network of fibers.

Pure CNC films can display very smooth surfaces [62], but as

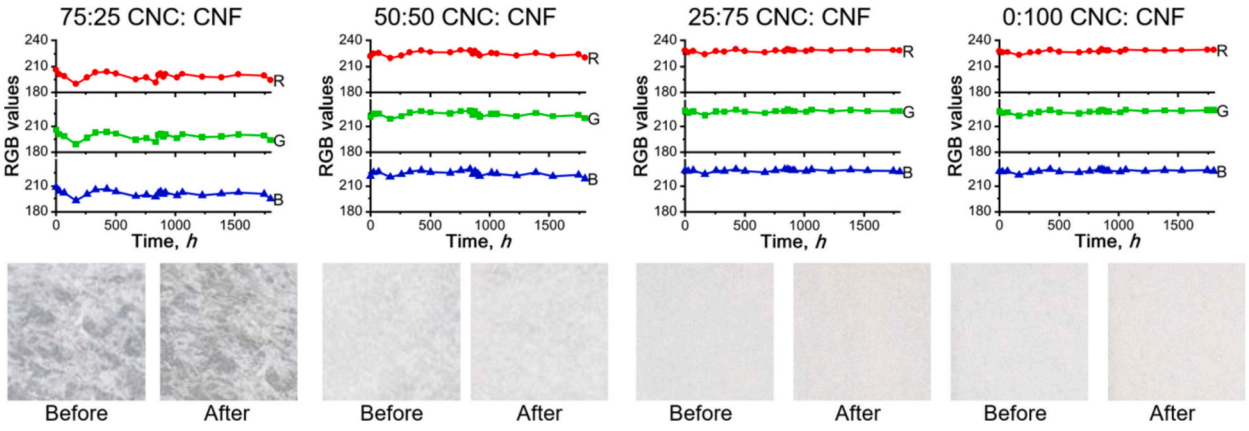

Fig. 9. RGB values over time for all-NC CNC: CNF films and their corresponding initial and final images after 1800 h of exposure.

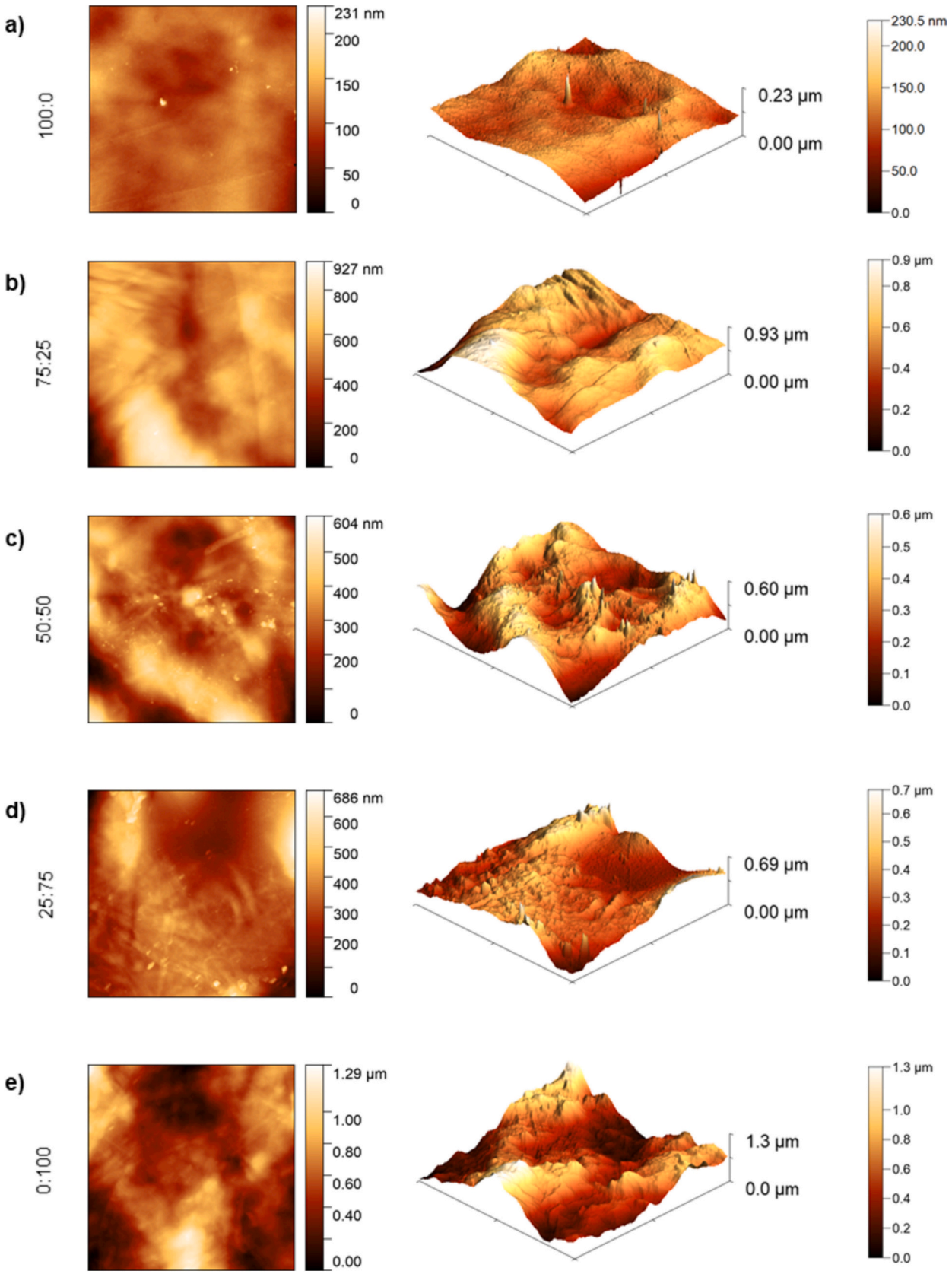

Fig. 10. AFM height images (left) and 3D surface images (right) of CNC: CNF films (25 μm^2 area).

discussed in this work, these films disintegrate when submerged in water and are much more challenging to handle than films with some CNF percentage. The addition of CNF ameliorates the mechanical properties of CNC films but significantly increases surface roughness.

The surface roughness of PET and PEN films was assessed for comparative analysis, considering their widespread application as substrates in printed electronic devices. The RMS roughness values consistently demonstrate that all tested cellulose films exhibit significantly higher roughness (4 to 34 times rougher) than PET and PEN films (Fig. S3). This heightened roughness in cellulose films can be attributed to their porous surface, which results from the uneven structure of the nanofibers, as well as their colloidal dimensions and imperfect packing. In our recent review on using bio-based materials in photovoltaics, we discussed the different approaches suggested in the literature to improve the smoothness of the surface of NC films [63].

3.8. General considerations: from packaging to photovoltaics

Unquestionably, the use of nanocellulose in cutting-edge applications is appealing due to its interesting optical properties, biodegradability, and renewability. In this work, we produce a range of multifunctional hybrid films with tunable properties that are suitable for various applications. For example, CNC: CNF: MTM films exhibit improved WVTR properties and significant resistance to swelling, making them ideal for packaging applications. Despite not having great WVTR values, it will be interesting in future work to assess whether the oxygen barrier of these films is similar to the high values obtained in pure cellulose nanomaterial films and, more importantly, whether the addition of MTM makes the oxygen barrier of these films less sensitive to humidity. Additionally, despite their low transparency, these films possess UV-blocking features, which could increase the lifetime of the goods packaged with these materials. Indeed, coffee and other highly sensitive products are packaged in light-blocking containers for this reason. However, the mechanical properties of these films are still below the industry standards required for this technology, which is why they are not expected to be used as a standalone technology but rather as a coating on a mechanically robust substrate, such as paper and board.

Alternatively, the CNC: CNF hybrid films without MTM exhibit noteworthy optical properties, including high transparency and tunable haze. Furthermore, their color stability under prolonged exposure to artificial sunlight makes them consistent for photovoltaic applications. The ability to adjust these materials' light scattering (haze) adds opportunities for anti-reflective or highly reflective surfaces. In this case, the CNC: CNF could be used as light management in photovoltaics, which requires long periods of light absorption and in protective systems against light effects. Nevertheless, these films need improvement in water resistance and further modification to be suitable for electronic systems, posing a challenge due to their higher roughness compared to PET and PEN. Here, future work around crosslinking and/or hydrophobization strategies may be necessary, but to retain the attractive optics, it is perhaps best that these treatments be applied *after* the film is formed so as not to disrupt the internal packing and organization that is responsible for the beneficial properties.

An essential characteristic of bio-based films is their biodegradability. This is a desirable property when this material is used for packaging due to environmental problems related to plastic packaging pollution. Photovoltaic technologies meant for indoor use, such as organic and perovskite solar cells, last only a few years [64]. These technologies are compatible with cellulose film substrates due to their low-temperature processing. One of their downsides is their sensitivity to moisture. Due to organic and perovskite solar cells' need for encapsulation to avoid performance loss and degradation, the biodegradability of cellulose films should not be an issue if they are isolated from degrading agents.

Indeed, NC hybrid films can be suitable for electronic systems only after depositing additional functional coatings to achieve all required characteristics [65]. Here, the NC films' roughness impacts the quality of subsequent layers deposited on top. In the realm of photovoltaics and other electronics applications, the deposition of functional layers is very susceptible to surface unevenness. There are successful cases of the deposition of conductive materials on NC films, such as ITO, [66,67] silver [68], copper [69] nanowires, and PEDOT: PSS [70], but all employed different deposition methods. For instance, atomic layer deposition and sputtering can result in very smooth and uniform layers; however, these methods are seldom used in mass production. While transparent and conductive layers can be deposited on cellulose with a low final surface roughness [71,72], this only applies to a sputtering deposition approach. More common methods of high-throughput production of perovskite solar cells are blade and slot-die coating, inkjet printing, and spray coating [73]. Solution methods require a smoother surface (RMS roughness <5 nm) [74]. While in slot-die coating, the substrate roughness has a negligible impact, and inkjet and spray deposition are very sensitive to topological unevenness [75]. NC films composed of CNF and partially made of CNC and CNF can be suitable for depositing transparent conductive layers via sputtering. However, a technique like slot-die casting would be more adequate in high-throughput production scenarios. Inkjet printing and spraying deposition methods would be restricted to pure CNC substrates due to their smooth surface until the surface roughness of CNC: CNF films is reduced, the possibility requiring a finer CNF quality.

4. Conclusions

In summary, CNC films properties can be significantly altered by the incorporation of CNF and MTM in their structure. The resulting hybrid films exhibited highly organized and dense structures, and their properties could be adjusted by varying the ratio of components. For instance, by incorporating MTM in CNC films, the water interactions are reduced and the original film easily dispersed in water retains its structure. The presence of CNF impacts more significantly the tensile properties of CNC films, and overall, MTM reduce the strength of films containing greater ratio CNF in their composition. There was no clear relationship between tensile properties and density. The films composed by CNC and CNF demonstrate different optical properties compared to those with just a single component. These changes become even more significant when the inorganic compound (MTM) was added to the film leading to a lower transparency. The variations in mechanical and optical properties observed in this research shows that by modifying the composition of films it is possible to customize and tailor of the films toward application-specific requirements. However, further reductions in moisture sensitivity will be necessary for high-performance applications since they often demand even lower levels of moisture absorption and interaction. All CNC: CNF composite films exhibited good UV stability (no visible degradation in 1000 h light soaking test under 1 Sun irradiation). Besides their bio-sourced origin, this makes them exciting substrates for packaging and sustainable solar energy and optoelectronic devices. Although their surface morphology (roughness 4–34 times higher compared to PEN and PET) can hinder the quality of subsequently deposited layers, different fabrication methods and treatments could ameliorate this constraint.

Abbreviations

CNC	Cellulose nanocrystals
CNF	Cellulose nanofibrils
MTM	Montmorillonite
PEN	Polyethylene naphthalate
PET	Polyethylene terephthalate
AFM	Atomic force microcopy
ITO	Indium tin oxide
PEDOT	Poly(3,4-ethylenedioxythiophene)
PSS	Polystyrene sulfonate

WVTR Water vapor transmission rate

CRediT authorship contribution statement

Joaquin Valdez Garcia: Writing – review & editing, Data curation. **Anna Boding:** Methodology, Investigation, Data curation. **Xuan Yang:** Writing – review & editing, Investigation. **Rustem Nizamov:** Writing – review & editing, Investigation. **Michael S. Reid:** Writing – review & editing, Investigation. **Kristina Junel:** Investigation. **Kati Miettunen:** Writing – review & editing, Supervision, Funding acquisition. **Tiffany Abitbol:** Writing – review & editing, Project administration, Funding acquisition, Conceptualization. **Joice Kaschuk:** Writing – review & editing, Writing – original draft, Formal analysis, Data curation.

Declaration of competing interest

The authors declare that they have no known competing financial interests or personal relationships that could have appeared to influence the work reported in this paper.

Acknowledgment

K.M., R.N. and J.V.G. thank the Academy of Finland (BioEST, project numbers 336577 and 336441). J.V.G. also thanks the University of Turku Graduate School UTUGS and Finnish Cultural Foundation for funding. T. A. acknowledges the Chair in Sustainable Materials at EPFL, co-funded by BASF, Logitech, Nestlé, and SIG, and funding from Formas for the "SUBSTAINABLE" project granted through the Tandem Forest Values program (Formas grant number 2019-02508).

Appendix A. Supplementary data

Supplementary data to this article can be found online at https://doi.org/10.1016/j.ijbiomac.2024.139203.

References

[1] R. Geyer, A brief history of plastics, in: Mare Plasticum - The Plastic Sea, Springer International Publishing, Cham, 2020, pp. 31–47, https://doi.org/10.1007/978-3-030-38945-1_2.
[2] T.R. Walker, L. Fequet, Current trends of unsustainable plastic production and micro(nano)plastic pollution, TrAC Trends Anal. Chem. 160 (2023) 116984, https://doi.org/10.1016/j.trac.2023.116984.
[3] T. Raj, K. Chandrasekhar, A. Naresh Kumar, S.H. Kim, Lignocellulosic biomass as renewable feedstock for biodegradable and recyclable plastics production: a sustainable approach, Renew. Sust. Energ. Rev. 158 (2022) 112130, https://doi.org/10.1016/J.RSER.2022.112130.
[4] Z. Fang, G. Hou, C. Chen, L. Hu, Nanocellulose-based films and their emerging applications, Curr. Opin. Solid State Mater. Sci. 23 (2019) 100764, https://doi.org/10.1016/j.cossms.2019.07.003.
[5] D. Hunter, Papermaking: The History and Technique of an Ancient Craft, Knopf, New York, 1943.
[6] Y. Wu, Y. Liang, C. Mei, L. Cai, A. Nadda, Q. Van Le, Y. Peng, S.S. Lam, C. Sonne, C. Xia, Advanced nanocellulose-based gas barrier materials: present status and prospects, Chemosphere 286 (2022) 131891, https://doi.org/10.1016/j.chemosphere.2021.131891.
[7] G. Dinesh, B. Kandasubramanian, Fabrication of transparent paper devices from nanocellulose fiber, Mater. Chem. Phys. 281 (2022) 125707, https://doi.org/10.1016/j.matchemphys.2022.125707.
[8] L. Solhi, V. Guccini, K. Heise, I. Solala, E. Niinivaara, W. Xu, K. Mihhels, M. Kröger, Z. Meng, J. Wohlert, H. Tao, E.D. Cranston, E. Kontturi, Understanding nanocellulose-water interactions: turning a detriment into an asset, Chem. Rev. (2022), https://doi.org/10.1021/acs.chemrev.2c00611.
[9] I. Leppänen, A. Hokkanen, M. Österberg, M. Vähä-Nissi, A. Harlin, H. Orelma, Hybrid films from cellulose nanomaterials—properties and defined optical patterns, Cellulose 29 (2022) 8551–8567, https://doi.org/10.1007/s10570-022-04795-0.
[10] D. Enescu, C. Gardrat, H. Cramail, C. Le Coz, G. Sèbe, V. Coma, Bio-inspired films based on chitosan, nanoclays and cellulose nanocrystals: structuring and properties improvement by using water-evaporation-induced self-assembly, Cellulose 26 (2019) 2389–2401, https://doi.org/10.1007/S10570-018-2211-7/FIGURES/6.
[11] W. Huang, Clay nanopapers, in: Nanopapers: From Nanochemistry and Nanomanufacturing to Advanced Applications, 2018, pp. 59–86, https://doi.org/10.1016/B978-0-323-48019-2.00003-7.
[12] L. Li, L. Maddalena, Y. Nishiyama, F. Carosio, Y. Ogawa, L.A. Berglund, Recyclable nanocomposites of well-dispersed 2D layered silicates in cellulose nanofibril (CNF) matrix, Carbohydr. Polym. 279 (2022) 119004, https://doi.org/10.1016/j.carbpol.2021.119004.
[13] L. Li, P. Chen, L. Medina, L. Yang, Y. Nishiyama, L.A. Berglund, Residual strain and nanostructural effects during drying of nanocellulose/clay Nanosheet hybrids: synchrotron X-ray scattering results, ACS Nano 17 (2023) 15810–15820, https://doi.org/10.1021/acsnano.3c03664.
[14] Y.C. Gorur, H.S. Francon, J. Sethi, L. Maddalena, C. Montanari, M.S. Reid, J. Erlandsson, F. Carosio, P.A. Larsson, L. Wågberg, Rapidly prepared nanocellulose hybrids as gas barrier, flame retardant, and energy storage materials, ACS Appl Nano Mater 5 (2022) 9188–9200, https://doi.org/10.1021/acsanm.2c01530.
[15] D. Xu, S. Wang, L.A. Berglund, Q. Zhou, Surface charges control the structure and properties of layered nanocomposite of cellulose nanofibrils and clay platelets, ACS Appl. Mater. Interfaces 13 (2021) 4463–4472, https://doi.org/10.1021/acsami.0c18594.
[16] M.L.C. de Oliveira, S. Mirmehdi, M.V. Scatolino, M.G. Júnior, A.R. Sanadi, R.A. P. Damasio, G.H.D. Tonoli, Effect of overlapping cellulose nanofibrils and nanoclay layers on mechanical and barrier properties of spray-coated papers, Cellulose 29 (2022) 1097–1113, https://doi.org/10.1007/S10570-021-04350-3/FIGURES/11.
[17] S.Y. Park, K. Lee, H. Shin, H.J. Youn, Eco-friendly flame retardant foam prepared by oven drying of pickering stabilized carboxymethylated cellulose nanofibril/nanoclay wet foam, Cellulose 29 (2022) 9693–9705, https://doi.org/10.1007/S10570-022-04867-1/FIGURES/6.
[18] P. Cazón, G. Velazquez, J.A. Ramírez, M. Vázquez, Polysaccharide-based films and coatings for food packaging: a review, Food Hydrocoll. 68 (2017) 136–148, https://doi.org/10.1016/j.foodhyd.2016.09.009.
[19] P. Subudhi, D. Punetha, Progress, challenges, and perspectives on polymer substrates for emerging flexible solar cells: a holistic panoramic review, Prog. Photovolt. Res. Appl. 31 (2023) 753–789, https://doi.org/10.1002/pip.3703.
[20] P. Ezati, A. Khan, R. Priyadarshi, T. Bhattacharya, S.K. Tammina, J.-W. Rhim, Biopolymer-based UV protection functional films for food packaging, Food Hydrocoll. 142 (2023) 108771, https://doi.org/10.1016/j.foodhyd.2023.108771.
[21] A. Sinha, J. Qian, S.L. Moffitt, K. Hurst, K. Terwilliger, D.C. Miller, L.T. Schelhas, P. Hacke, UV-induced degradation of high-efficiency silicon PV modules with different cell architectures, Prog. Photovolt. Res. Appl. 31 (2023) 36–51, https://doi.org/10.1002/pip.3606.
[22] X. Li, N. Wang, X. Zhang, H. Chang, Y. Wang, Z. Zhang, Optical haze regulation of cellulose nanopaper via morphological tailoring and nano-hybridization of cellulose nanoparticles, Cellulose 27 (2020) 1315–1326, https://doi.org/10.1007/s10570-019-02876-1.
[23] M. Kim, S. Kim, N. Han, S. Lee, H. Kim, Understanding viscoelastic behavior of hybrid nanocellulose film based on rheological and electrostatic observation in blended suspension, Carbohydr. Polym. 300 (2023) 120218, https://doi.org/10.1016/j.carbpol.2022.120218.
[24] Y. Hua, T. Chen, Y. Tang, Preparation and characterization of nanocomposite films based on different ratios of cellulose nanocrystal and cellulose nanofiber, Ind. Crop. Prod. 179 (2022) 114686, https://doi.org/10.1016/j.indcrop.2022.114686.
[25] C.Q. Pritchard, G. Funk, J. Owens, S. Stutz, A. Gooneie, J. Sapkota, E.J. Foster, M. J. Bortner, Adjustable film properties of cellulose nanofiber and cellulose nanocrystal composites, Carbohydr. Polym. 286 (2022) 119283, https://doi.org/10.1016/j.carbpol.2022.119283.
[26] M.S. Reid, M. Villalobos, E.D. Cranston, Benchmarking cellulose nanocrystals: from the laboratory to industrial production, Langmuir 33 (2017) 1583–1598, https://doi.org/10.1021/acs.langmuir.6b03765.
[27] L. Wågberg, G. Decher, M. Norgren, T. Lindström, M. Ankerfors, K. Axnäs, The build-up of polyelectrolyte multilayers of microfibrillated cellulose and cationic polyelectrolytes, Langmuir 24 (2008) 784–795, https://doi.org/10.1021/LA702481V/SUPPL_FILE/LA702481V-FILE002.PDF.
[28] T. Abitbol, A. Ahniyaz, R. Álvarez-Asencio, A. Fall, A. Swerin, Nanocellulose-based hybrid materials for UV blocking and mechanically robust barriers, ACS Appl. Bio Mater. 3 (2020) 2245–2254, https://doi.org/10.1021/acsabm.0c00058.
[29] A. Poskela, K. Miettunen, A. Tiihonen, P.D. Lund, Extreme sensitivity of dye solar cells to UV-induced degradation, Energy Sci. Eng. 9 (2021), https://doi.org/10.1002/ese3.810.
[30] T. Abitbol, M. Kubat, E. Brännvall, N. Kotov, C.M. Johnson, R. Nizamov, M. Nyberg, K. Miettunen, N. Nordgren, J.S. Stevanic, M.P. Guerreiro, Isolation of mixed compositions of cellulose nanocrystals, microcrystalline cellulose, and lignin nanoparticles from wood pulps, ACS, Omega 8 (2023) 21474–21484, https://doi.org/10.1021/acsomega.3c00295.
[31] A. Lawrynowicz, E. Palo, R. Nizamov, K. Miettunen, Self-cleaning and UV-blocking cotton – fabricating effective ZnO structures for photocatalysis, J. Photochem. Photobiol. A Chem. 450 (2024) 115420, https://doi.org/10.1016/j.jphotochem.2023.115420.
[32] K.L. Spence, R.A. Venditti, Y. Habibi, O.J. Rojas, J.J. Pawlak, The effect of chemical composition on microfibrillar cellulose films from wood pulps: mechanical processing and physical properties, Bioresour. Technol. 101 (2010) 5961–5968, https://doi.org/10.1016/j.biortech.2010.02.104.
[33] S. Abend, G. Lagaly, Sol–gel transitions of sodium montmorillonite dispersions, Appl. Clay Sci. 16 (2000) 201–227, https://doi.org/10.1016/S0169-1317(99)00040-X.
[34] Q. Yang, C.-N. Wu, T. Saito, A. Isogai, Cellulose–clay layered nanocomposite films fabricated from aqueous cellulose/LiOH/urea solution, Carbohydr. Polym. 100 (2014) 179–184, https://doi.org/10.1016/j.carbpol.2012.10.044.
[35] L. Alves, A. Ramos, E. Ferraz, P. Sanguino, J. Santarén, M.G. Rasteiro, J.A. F. Gamelas, Effect of the dispersion state of minerals on the properties of cellulose

nanofiber-based composite films, Appl. Clay Sci. 233 (2023) 106823, https://doi.org/10.1016/j.clay.2023.106823.
[36] J.J. Kaschuk, Y. Al Haj, J. Valdez Garcia, A. Kamppinen, O.J. Rojas, T. Abitbol, K. Miettunen, J. Vapaavuori, Processing factors affecting roughness, optical and mechanical properties of nanocellulose films for optoelectronics, Carbohydr. Polym. 332 (2024) 121877, https://doi.org/10.1016/j.carbpol.2024.121877.
[37] F. Chen, W. Xiang, D. Sawada, L. Bai, M. Hummel, H. Sixta, T. Budtova, Exploring large ductility in cellulose nanopaper combining high toughness and strength, ACS Nano 14 (2020) 11150–11159, https://doi.org/10.1021/acsnano.0c02302.
[38] T. Guo, L. Gu, Y. Zhang, H. Chen, B. Jiang, H. Zhao, Y. Jin, H. Xiao, Bioinspired self-assembled films of carboxymethyl cellulose–dopamine/montmorillonite, J Mater Chem A Mater 7 (2019) 14033–14041, https://doi.org/10.1039/C9TA00998A.
[39] B. Natarajan, A. Krishnamurthy, X. Qin, C.D. Emiroglu, A. Forster, E.J. Foster, C. Weder, D.M. Fox, S. Keten, J. Obrzut, J.W. Gilman, Binary cellulose nanocrystal blends for bioinspired damage tolerant photonic films, Adv. Funct. Mater. 28 (2018) 1800032, https://doi.org/10.1002/adfm.201800032.
[40] C. Hu, Y. Zhou, T. Zhang, T. Jiang, C. Meng, G. Zeng, Morphological, thermal, mechanical, and optical properties of hybrid nanocellulose film containing cellulose nanofiber and cellulose nanocrystals, Fibers and Polymers 22 (2021) 2187–2193, https://doi.org/10.1007/s12221-021-0903-3.
[41] X. Sun, Q. Wu, X. Zhang, S. Ren, T. Lei, W. Li, G. Xu, Q. Zhang, Nanocellulose films with combined cellulose nanofibers and nanocrystals: tailored thermal, optical and mechanical properties, Cellulose 25 (2018) 1103–1115, https://doi.org/10.1007/s10570-017-1627-9.
[42] X. Yang, L. Li, Y. Nishiyama, M.S. Reid, L.A. Berglund, Processing strategy for reduced energy demand of nanostructured CNF/clay composites with tailored interfaces, Carbohydr. Polym. 312 (2023) 120788, https://doi.org/10.1016/j.carbpol.2023.120788.
[43] C.-N. Wu, T. Saito, S. Fujisawa, H. Fukuzumi, A. Isogai, Ultrastrong and high gas-barrier nanocellulose/clay-layered composites, Biomacromolecules 13 (2012) 1927–1932, https://doi.org/10.1021/bm300465d.
[44] L. Medina, Y. Nishiyama, K. Daicho, T. Saito, M. Yan, L.A. Berglund, Nanostructure and properties of nacre-inspired clay/cellulose nanocomposites—synchrotron X-ray scattering analysis, Macromolecules 52 (2019) 3131–3140, https://doi.org/10.1021/acs.macromol.9b00333.
[45] A. Liu, L.A. Berglund, Clay nanopaper composites of nacre-like structure based on montmorrilonite and cellulose nanofibers—improvements due to chitosan addition, Carbohydr. Polym. 87 (2012) 53–60, https://doi.org/10.1016/j.carbpol.2011.07.019.
[46] R. Masoodi, A. Javadi, K. Pillai, R. Sabo, An experimental study on swelling of cellulose nano-fiber films in epoxy resins and water, in: International SAMPE Technical Conference, 2011.
[47] C. Palasingh, A. Ström, H. Amer, T. Nypelö, Oxidized xylan additive for nanocellulose films – a swelling modifier, Int. J. Biol. Macromol. 180 (2021) 753–759, https://doi.org/10.1016/j.ijbiomac.2021.03.062.
[48] S. Shrestha, J.A. Diaz, S. Ghanbari, J.P. Youngblood, Hygroscopic swelling determination of cellulose nanocrystal (CNC) films by polarized light microscopy digital image correlation, Biomacromolecules 18 (2017) 1482–1490, https://doi.org/10.1021/acs.biomac.7b00026.
[49] C. Aulin, G. Salazar-Alvarez, T. Lindström, High strength, flexible and transparent nanofibrillated cellulose–nanoclay biohybrid films with tunable oxygen and water vapor permeability, Nanoscale 4 (2012) 6622, https://doi.org/10.1039/c2nr31726e.
[50] L. Alves, E. Ferraz, J.A.F. Gamelas, Composites of nanofibrillated cellulose with clay minerals: a review, Adv. Colloid Interf. Sci. 272 (2019) 101994, https://doi.org/10.1016/j.cis.2019.101994.
[51] J.J. Kaschuk, Y. Al Haj, O.J. Rojas, K. Miettunen, T. Abitbol, J. Vapaavuori, Plant-based structures as an opportunity to engineer optical functions in next-generation light management, Adv. Mater. 34 (2022) 2104473, https://doi.org/10.1002/adma.202104473.
[52] Z. Fang, H. Zhu, Y. Yuan, D. Ha, S. Zhu, C. Preston, Q. Chen, Y. Li, X. Han, S. Lee, G. Chen, T. Li, J. Munday, J. Huang, L. Hu, Novel nanostructured paper with ultrahigh transparency and ultrahigh haze for solar cells, Nano Lett. 14 (2014) 765–773, https://doi.org/10.1021/nl404101p.
[53] A. Tiihonen, K. Miettunen, J. Halme, S. Lepikko, A. Poskela, P.D. Lund, Critical analysis on the quality of stability studies of perovskite and dye solar cells, Energy, Environ. Sci. 11 (2018) 730–738, https://doi.org/10.1039/C7EE02670F.
[54] T. Watson, P. Holliman, D. Worsley, Rapid, continuous in situ monitoring of dye sensitisation in dye-sensitized solar cells, J. Mater. Chem. 21 (2011) 4321, https://doi.org/10.1039/c0jm03607b.
[55] M.L. Davies, T.M. Watson, P.J. Holliman, A. Connell, D.A. Worsley, In situ monitoring and optimization of room temperature ultra-fast sensitization for dye-sensitized solar cells, Chem. Commun. 50 (2014) 12512–12514, https://doi.org/10.1039/C4CC05766J.
[56] L. Furnell, P.J. Holliman, A. Connell, E.W. Jones, R. Hobbs, C.P. Kershaw, R. Anthony, J. Searle, T. Watson, J. McGettrick, Digital imaging to simultaneously study device lifetimes of multiple dye-sensitized solar cells, Sustain, Energy Fuel 1 (2017) 362–370, https://doi.org/10.1039/C7SE00015D.
[57] A. Poskela, A. Tiihonen, H. Palonen, P.D. Lund, K. Miettunen, Predictive modeling of dye solar cell degradation, Sol. RRL 6 (2022), https://doi.org/10.1002/solr.202101004.
[58] C.R. Osterwald, T.J. McMahon, History of accelerated and qualification testing of terrestrial photovoltaic modules: a literature review, Prog. Photovolt. Res. Appl. 17 (2009) 11–33, https://doi.org/10.1002/pip.861.
[59] A. Tiihonen, V. Siipola, K. Lahtinen, H. Pajari, P. Widsten, T. Tamminen, T. Kallio, K. Miettunen, Biocarbon from brewery residues as a counter electrode catalyst in dye solar cells, Electrochim. Acta 368 (2021) 137583, https://doi.org/10.1016/j.electacta.2020.137583.
[60] J. Kaschuk, R. Nizamov, Y. Al Haj, M. Nyberg, I. Monireh, E. Pasquier, O.J. Rojas, K. Miettunen, T. Abitbol, J. Vapaavuori, Stability of Nanocellulose Films Under Artificial Sunlight Exposure Toward Sustainable Optoelectronics Substrates, 2024 (Submitted).
[61] K.W. Klockars, N.E. Yau, B.L. Tardy, J. Majoinen, T. Kämäräinen, K. Miettunen, E. Boutonnet, M. Borghei, J. Beidler, O.J. Rojas, Asymmetrical coffee rings from cellulose nanocrystals and prospects in art and design, Cellulose 26 (2019) 491–506, https://doi.org/10.1007/s10570-018-2167-7.
[62] Y. Zhou, C. Fuentes-Hernandez, T.M. Khan, J.-C. Liu, J. Hsu, J.W. Shim, A. Dindar, J.P. Youngblood, R.J. Moon, B. Kippelen, Recyclable organic solar cells on cellulose nanocrystal substrates, Sci. Rep. 3 (2013) 1536, https://doi.org/10.1038/srep01536.
[63] K. Miettunen, M. Hadadian, J.V. García, A. Lawrynowicz, E. Akulenko, O.J. Rojas, M. Hummel, J. Vapaavuori, Bio-based materials for solar cells, WIREs Energy and Environment 13 (2024), https://doi.org/10.1002/wene.508.
[64] M. Seri, F. Mercuri, G. Ruani, Y. Feng, M. Li, Z.-X. Xu, M. Muccini, Toward real setting applications of organic and perovskite solar cells: a comparative review, Energ. Technol. 9 (2021), https://doi.org/10.1002/ente.202000901.
[65] W. Liu, K. Liu, H. Du, T. Zheng, N. Zhang, T. Xu, B. Pang, X. Zhang, C. Si, K. Zhang, Cellulose nanopaper: fabrication, functionalization, and applications, Nanomicro Lett 14 (2022) 104, https://doi.org/10.1007/s40820-022-00849-x.
[66] M.A.H. Khondoker, S.Y. Yang, S.C. Mun, J. Kim, Flexible and conductive ITO electrode made on cellulose film by spin-coating, Synth. Met. 162 (2012) 1972–1976, https://doi.org/10.1016/j.synthmet.2012.09.005.
[67] C. Legnani, H.S. Barud, J.M.A. Caiut, V.L. Calil, I.O. Maciel, W.G. Quirino, S.J. L. Ribeiro, M. Cremona, Transparent bacterial cellulose nanocomposites used as substrate for organic light-emitting diodes, J. Mater. Sci. Mater. Electron. 30 (2019) 16718–16723, https://doi.org/10.1007/s10854-019-00979-w.
[68] P.-C. Lin, C.-T. Hsieh, X. Liu, F.-C. Chang, W.-C. Chen, J. Yu, C.-C. Chueh, Fabricating efficient flexible organic photovoltaics using an eco-friendly cellulose nanofibers/silver nanowires conductive substrate, Chem. Eng. J. 405 (2021) 126996, https://doi.org/10.1016/j.cej.2020.126996.
[69] J. Sun, X. Li, Z. Chen, S. Yan, L. Qin, J. Zeng, S. Wang, J. Xu, L. Zhao, W. Zhou, Q. Wang, H. Gong, A. Lu, J. Yu, Copper nanowires/cellulose biodegradable flexible transparent conductor with improved thermal stability and its application, Org. Electron. 63 (2018) 392–397, https://doi.org/10.1016/j.orgel.2018.09.020.
[70] Y. Ko, D. Kim, U.-J. Kim, J. You, Vacuum-assisted bilayer PEDOT:PSS/cellulose nanofiber composite film for self-standing, flexible, conductive electrodes, Carbohydr. Polym. 173 (2017) 383–391, https://doi.org/10.1016/j.carbpol.2017.05.096.
[71] X. Liu, K. Huang, X. Lin, H. Li, T. Tao, Q. Wu, Q. Zheng, L. Huang, Y. Ni, L. Chen, X. Ouyang, J. Li, Transparent and conductive cellulose film by controllably growing aluminum doped zinc oxide on regenerated cellulose film, Cellulose 27 (2020) 4847–4855, https://doi.org/10.1007/s10570-020-03147-0.
[72] X. Liu, W. Xiao, T. Tao, J. Yang, H. Li, Q. Chen, L. Huang, Y. Ni, L. Chen, X. Ouyang, X. Zhu, J. Li, Transparent, smooth, and sustainable cellulose-derived conductive film applied for the flexible electronic device, Carbohydr. Polym. 260 (2021) 117820, https://doi.org/10.1016/j.carbpol.2021.117820.
[73] Y. Wang, C. Duan, P. Lv, Z. Ku, J. Lu, F. Huang, Y.-B. Cheng, Printing strategies for scaling-up perovskite solar cells, Natl Sci Rev 8 (2021) nwab075. doi:https://doi.org/10.1093/nsr/nwab075.
[74] H. Yu, D. Fang, M. Dirican, R. Wang, Y. Tian, L. Chen, H. Liu, J. Wang, F. Tang, A. M. Asiri, X. Zhang, J. Tao, Binding conductive ink initiatively and strongly: transparent and thermally stable cellulose nanopaper as a promising substrate for flexible electronics, ACS Appl. Mater. Interfaces 11 (2019) 20281–20290, https://doi.org/10.1021/acsami.9b04596.
[75] X. Peng, J. Yuan, S. Shen, M. Gao, A.S.R. Chesman, H. Yin, J. Cheng, Q. Zhang, D. Angmo, Perovskite and organic solar cells fabricated by inkjet printing: progress and prospects, Adv. Funct. Mater. 27 (2017) 1703704, https://doi.org/10.1002/adfm.201703704.